Proceedings of the Pakistan Academy of Sciences: A Physical and Computational Sciences 62(1): 81-95 (2025)
Copyright © Pakistan Academy of Sciences
ISSN (Print): 2518-4245; ISSN (Online): 2518-4253
http://doi.org/10.53560/PPASA(62-1)869

Pakistan Academy of Sciences

Research Article

A Study on CIGS Thin-Film Solar Cells Through SCAPS-1D Simulations

Ateeq ul Rehman[1], Shahbaz Afzal[2], Iqra Naeem[1], Tahir Munir[1], Sakhi Ghulam Sarwar[3], Muhammad Saleem[1], and Raphael M. Obodo[4*]

[1]Institute of Physics, Baghdad ul Jadeed Campus, The Islamia University of Bahawalpur, Bahawalpur, Pakistan
[2]Department of Physics, University of Education Lahore, D.G. Khan Campus, Pakistan
[3]Centre of Excellence in Solid-State Physics, University of the Punjab, Lahore, Pakistan
[4]Department of Physics and Astronomy, University of Nigeria, Nsukka, Enugu State, Nigeria

Abstract: This research utilized SCAPS-1D simulation software to model a high-efficiency CIGS-based solar cell with configuration Ag/ZnO:Al/i-ZnO/CdS/CIGS/Mo. Various optimizations were performed, focusing on the absorber layer's thickness, defect density, and acceptor density to enhance the cell's performance. Moreover, the work function values of rear contact metals were studied in regard to their effect on important V_{oc}, J_{sc}, FF, and PCE steps in critical photovoltaics parameters. Their Influence was compared alongside temperature, highlighting the importance of reliable thermal control systems for sustained performance under changing conditions. The study further emphasized the importance of the hole transport layer (HTL) in improving charge carrier collection and reducing recombination losses. Efforts to develop cadmium-free designs reinforced the push towards sustainable and eco-friendly photovoltaic technologies. The optimal parameters achieved in this study included an absorber layer thickness of 0.4 µm, acceptor density of absorber at 1×10^{18} cm^{-3}, defect density of 1×10^{15} cm^{-3}, and a back contact selenium work function of 5.9 eV. Under AM 1.5 G spectrum illumination at 300 K, the optimized cell demonstrated exceptional performance, with a V_{oc} of 0.7338 V, J_{sc} of 36.352805 mA/cm^2, FF of 83.33%, and PCE of 22.23%. The results were benchmarked against existing literature, showcasing significant improvements in device efficiency. This study provides a comprehensive framework for optimizing CIGS-based solar cells and highlights their potential for delivering high-performance, sustainable solar energy.

Keywords: SCAPS 1D, Thin Films, Solar Cell, CIGS, Simulations.

1. INTRODUCTION

For last many years, scientists have devoted considerable resources to investigating renewable energy sources as sustainable alternatives to fossil fuels primarily due to their finite availability and significant environmental impact. Fossil fuels release substantial quantities of carbon dioxide, a greenhouse gas that significantly contributes to the expedited progression of climate change. Furthermore, the extraction and consumption of these finite resources result in significant environmental deterioration, encompassing air and water contamination. At the same time, their restricted availability engenders apprehensions regarding the sustainability of energy resources in the long term [1-3]. Photovoltaic (PV) energy has emerged as a promising solution for pursuing a sustainable and more environmentally friendly future [4-5]. PV technology focuses on converting sunlight into electrical energy, offering the potential to reduce dependence on finite fossil fuels, mitigate greenhouse gas emissions, and facilitate a shift toward clean, renewable energy sources [6]. Consequently, renewable energy has increasingly focused on materials that have high

---

Received: June 2024; Revised: February 2025; Accepted: March 2025
* Corresponding Author: Raphael M. Obodo <Raphael.obodo@unn.edu.ng>

energy conversion efficiency with environmentally sustainable [7]. Ongoing research and development efforts have increasingly focused on cells composed of III-VI materials like InSe, GaSe, and GaS, demonstrating significant potential for advancing solar energy production while maintaining environmental sustainability. A key consideration in this field is optimizing the efficiency-to-cost ratio, a crucial factor driving the advancement of thin-film solar cell materials. Chalcopyrite-based solar cells typically feature a substantial absorbent layer (up to 2 μm in thickness), capable of efficiently capturing a vast portion of the solar spectrum. Chalcogenide photovoltaic technologies, as a novel alternative to conventional silicon-based systems, offer exciting opportunities for advancing solar cell performance and cost-effectiveness [8-10].

The continuous progress in thin-film solar cell technology has attracted significant scholarly interest in recent years, especially concerning enhancing materials like Copper Indium Gallium Selenide (CIGS). Numerous studies have demonstrated the potential of CIGS-based solar cells to attain elevated power conversion efficiencies (PCE) while addressing the challenges of cost and scalability. For instance, Abdulmageed *et al.* [11] verified that CIGS solar cells can achieve PCE values exceeding 20% under laboratory conditions Specifically, Islam *et al*. [12] work with a CIGS absorber layer having a thickness of 1 μm has been shown to reach an efficiency of approximately 17% while Das *et al.* [13] laboratory-reported efficiencies range between 12% and 13%.

Notably, the study by Goncalves *et al*. [14] explored the effect of reducing the thickness of the CIGS absorber layer, demonstrating the potential for achieving theoretical efficiencies as high as 33%. Despite these remarkable results, the widespread adoption of CIGS thin-film solar cells remains constrained by the high cost of indium and gallium. However, their unique attributes, such as tunable band gaps, high absorption coefficients, and excellent external stability, continue to position CIGS cells as a promising contender for next-generation photovoltaic technologies [15]. Recent studies have further refined the performance of CIGS devices by optimizing material parameters. For example, Hossain *et al.* [16] achieved a PCE of 23% by optimizing various CIGS parameters. Danladi *et al.* [17] reported an efficiency of 22.58% through similar optimization efforts. In addition to the previous studies, other scholars have concentrated on augmenting the scalability and cost-effectiveness of devices based on Copper Indium Gallium Selenide (CIGS). For example, Muzakkar *et al.* [18] examined innovative doping methodologies to improve carrier mobility and the overall efficacy of the devices. Likewise, Smith *et al.* [19] investigated alternative fabrication techniques to mitigate dependence on indium while maintaining optimal performance. These synergistic endeavors underscore the persistent advancements achieved to elevate the efficiency and economic viability of CIGS thin-film solar cells, reinforcing their significance in the shift toward sustainable energy solutions.

This study proposes a novel CIGS-based solar cell structure with Cadmium Sulfide (CdS) as a buffer layer. This material is widely adopted in thin-film solar cells due to its favorable properties. The use of CDs offers several advantages, including efficient charge carrier separation, excellent optical properties, chemical stability, tunability, cost-effectiveness, and compatibility with various deposition techniques, making it a preferred choice for enhancing the performance and reliability of CIGS-based photovoltaic devices [20, 21]. The proposed Ag/ZnO:Al/i-ZnO/CdS/CIGS/Mo solar cell model was comprehensively analyzed, exploring various parameters to optimize its performance and implementation. Key factors, such as the thickness of the absorber, acceptor density, and defect densities, were systematically varied to understand their impact on power conversion efficiency (PCE) and overall device stability. Additionally, the study evaluated the influence of rear contact materials, operating temperatures, different hole transport layers HTLs, and alternative buffer layers to identify the most effective configuration for achieving enhanced photovoltaic performance. Prior studies have demonstrated the potential of CIGS solar cells, but limited attention has been given to exploring alternative buffer materials such as SnS_2, In_2S_3, and ZnSe, as well as different hole transport layers (HTLs) like CuI and Spiro-OMeTAD, and rear contact materials. This study is distinguished by its methodical optimization of the structural parameters inherent to the CIGS solar cell, aimed at realizing elevated efficiencies alongside economic efficiency. Innovative features encompass the incorporation of CdS as the buffer layer and the subsequent assessment of its influence on the comprehensive photovoltaic performance. The results yield critical insights into the architecture of high-performance CIGS-based solar cells that possess practical scalability and economic feasibility. Prospective research trajectories will emphasize the amalgamation of advanced materials with CIGS-based frameworks to augment efficiency and stability further. Furthermore, initiatives will be concentrated on formulating cost-effective and environmentally sustainable fabrication methodologies to promote the extensive implementation of CIGS thin-film solar cells within the renewable energy landscape.

2. METHODOLOGY

The utilization of SCAPS 1D in this simulation study is based on the one-dimensional solar cell capacitance program created and upheld by Marc Burgelman and his research team at the Department of Electronics and Information Systems at the University of Ghent in Belgium [15]. SCAPS 1-D functions by solving key semiconductor equations, which include the Poisson equation, continuity equations for electrons and holes as shown in Equations (1-3) [22-24].

$$\frac{d^2}{dx^2}\varphi(x) = \frac{e}{\varepsilon_0\varepsilon_r}\rho(x) - n(x) + N_D - N_A + \rho_P\rho_N \quad (1)$$

$$-\left(\frac{1}{q}\right)\frac{\partial J_P}{dx} + \mathrm{U}_P + G = \frac{\partial P}{\partial t} \quad (2)$$

$$-\left(\frac{1}{q}\right)\frac{\partial J_n}{dx} + \mathrm{U}_n + G = \frac{\partial n}{\partial t} \quad (3)$$

Where, $\varphi(x)$ denotes the electrostatic potential, *e* represents the elementary charge, ε_r stands for relative permittivity, ε_0 is the vacuum permittivity, *p* and *n* indicate concentrations of holes and electrons, N_A and N_D are for acceptor and donor densities respectively. Additionally, ρ_n and ρ_p describe electron and hole distributions, while J_n and J_p represent current densities for electrons and holes. *G* signifies the carrier generation rate in Equations (2) and (3).

2.1. Materials and Layer Details

The solar cell architecture investigated in his research comprises multiple layers, each serving a distinct purpose in optimizing device performance. The primary materials used in the solar cells include: soda-lime glass substrate provides mechanical support for the solar cell structure. Molybdenum (Mo) is employed as the back contact due to its excellent electrical properties and thermal stability. The absorber layer, composed of Copper Indium Gallium Selenide (CIGS), is the key sunlight absorber and is vibrant in converting photons into charge carriers. The Cadmium Sulfide (CdS) buffer layer is crucial for aligning the energy bands and facilitating efficient charge carrier transport among the absorber and window layer. To address environmental concerns, alternative buffer materials like Tin disulfide (SnS_2), Indium Sulfide (In_2S_3), and Zinc Selenide (ZnSe) are suggested to substitute CdS due to concerns regarding cadmium in solar cells. Furthermore, Intrinsic Zinc Oxide (i-ZnO) is used as a window layer to improve light scattering and increase photon absorption. The transparent conducting oxide (TCO) layer consists of Aluminum-doped Zinc Oxide (ZnO:Al), which improves electrical conductivity and reduces sheet resistance. Additional materials such as Copper Iodide (CuI) and Spiro-OMeTAD are examined as hole transport layers (HTLs) to enhance charge carrier collection and reduce recombination losses [25, 26].

2.2. Solar Cell Construction

The architecture of the solar cell is designed as Ag/ZnO:Al/i-ZnO/CdS/CIGS/Mo, with layers constructed sequentially on a sod-lime glass substrate. The Molybdenum (Mo) back contact layer is deposited first, providing a stable base for the subsequent layer and ensuring good electrical contact. Next, the CIGS absorber layer is deposited, followed by the CdS buffer layer, which ensures proper band alignment for efficient charge transport. Intrinsic Zinc Oxide (i-ZnO) is then applied as the window layer to optimize the light scattering and absorption. The Aluminum-doped Zinc Oxide (ZnO:Al) TCO layer, with a thickness of 500 nm, is added on top to enhance conductivity and improve carrier mobility. Finally, Silver (Ag) is applied as the front contact to complete the structure. The proposed design also incorporates modifications to address cadmium-related concerns by substituting buffer materials such as SnS_2, In_2S_3, and ZnSe and incorporating CuI and Spiro-oMeTAD as hole transport layers. These modifications aim to improve solar cell performance and sustainability, as shown in Figure 1. The intrinsic properties of each layer are defined by assigning explicit defects to their particular elements, as outlined in Tables (1-3).

3. RESULTS AND DISCUSSION

3.1. Mechanism of Solar Cells

Solar cells operate on the principle of the photovoltaic effect, which is the generation of electric current when a material captivates light energy. The process begins when sunlight illuminates the solar cell. Photons with energies equal to or greater than the bandgap energy of the absorber material (such as CIGS in this study) are absorbed, exciting electrons from the valence band to the conduction band. This excitation creates electron-hole pairs, which are the fundamental charge carriers in the solar cell [27]. A PN junction is employed in the solar cell structure to couple the energy of these charge carriers. The PN junction creates an internal electric field that separates the electron-hole pairs. Electrons are driven towards the N-type layer, while holes are pushed towards the P-type layer. This separation prevents recombination of the charges and allows them to move towards their respective electrodes. The front and back contacts of the solar cell collect the electrons and holes. The collected electrons flow through an external circuit, creating an electric current, while the holes flow to the back contact to complete the circuit. Several factors, including the material properties, the thickness of the absorber layer, the defect density, and the alignment of energy bands between the layers, influence the efficiency of this process. The role of the transparent conducting oxide (TCO), such as ZnO:Al, is to allow sunlight to pass through to the absorber layer while facilitating the movement of charge carriers. The buffer layer, such as CdS or cadmium-free alternatives like In_2S_3, aligns the energy bands between the absorber and the TCO, ensuring efficient charge transport. The back contact, such as molybdenum (Mo), facilitates the collection of holes and ensures good ohmic contact with the absorber layer [11-15, 28].

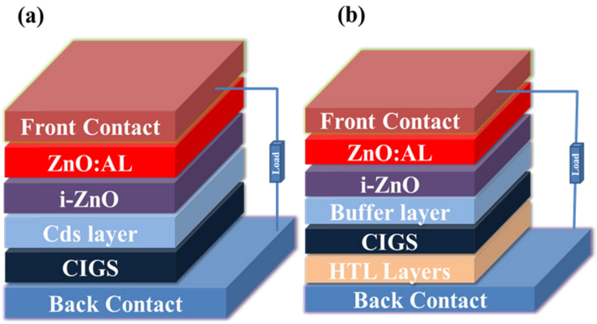

Fig. 1. (a) CIGS-based-simulated fundamental structure of solar cells, (b) CIGS-based solar cell with different buffer and hole layers.

This investigation presents an innovative solar cell architecture designated as Ag/ZnO:Al/i-ZnO/CdS/CIGS/Mo, which, following an extensive review of existing literature, appears to be unreported in the context of comparative analysis. The originality of this research is manifested in its benchmarking of performance metrics against other established configurations, such as Ag/ZnO:Al/ZnO/CdS/Sb_2Se_3/Mo, which attained a power conversion efficiency (PCE) of 8.72%, and CdS/Sb_2Se_3/Mo/

Table 1. Different used simulation parameters.

S. No.	Electrical Parameter	CIGS [25]	CdS [5]	i-ZnO [5]	ZnO:AI [5]
1	Bandgap (eV)	1.2	2.4	3.3	3.3
2	Dielectric permittivity (eV)	13.6	10	9	9
3	Thickness (μm)	2	0.05	0.05	0.5
4	CB (cm^{-3})	2.2×10^{18}	2.2×10^{18}	2.2×10^{18}	2.2×10^{18}
5	VB (cm^{-3})	1.8×10^{19}	1.8×10^{19}	1.8×10^{19}	1.8×10^{19}
6	Electron affinity (eV)	4.5	4.2	4.45	4.45
7	Electron mobility (cm^2/Vs)	1×10^2	1×10^2	1×10^2	1×10^2
8	Hole mobility (cm^2/Vs)	2.5×10^1	2.5×10^1	2.5×10^1	2.5×10^1
9	N_D (cm^{-3})	0	1×10^{17}	1×10^{15}	1×10^{18}
10	N_A (cm^{-3})	1×10^{16}	1×10^2	1×10^1	1×10^1
11	N_t (cm^{-3})	1×10^{15}	1×10^{15}	1×10^{10}	1×10^{17}

Table 2. Parameters of additional Buffer and Hole transport layer.

S. No.	Parameter	ZnSe [5]	SnS_2 [5]	In_2S_3 [5]	Spiro-Metad [26]	CuI [26]
1	Bandgap (eV)	2.4	2.45	2.8	3	3.1
2	CB (cm^{-3})	2.2×10^{18}	7.32×10^{18}	1.8×10^{19}	2.8×10^{18}	2.8×10^{19}
3	VB (cm^{-3})	1.8×10^{19}	1×10^{19}	4×10^{18}	1.8×10^{10}	1×10^{19}
4	Dielectric permittivity (eV)	10	17.7	13.5	3	6.5
5	Electron affinity (eV)	4.2	4.26	4.7	2.2	2.1
6	Thickness (μm)	0.05	0.05	0.025	0.2	0.1
7	N_D (cm^{-3})	1×10^{17}	9.85×10^{18}	1×10^{22}	0	0
8	N_A (cm^{-3})	1×10^{2}	0	0	1×10^{18}	1×10^{18}
9	Electron mobility (cm^2/Vs)	1×10^{2}	2.5×10^{1}	4×10^{2}	2.1×10^{-3}	1×10^{2}
10	Hole mobility (cm^2/Vs)	2.5×10^{2}	5×10^{1}	2.1×10^{2}	2.16×10^{-3}	4.39×10^{11}
11	Defect density (N_t)	1×10^{14}	1×10^{15}	1×10^{14}	1×10^{15}	1×10^{15}

Table 3. Front and Back contact values [29].

Electrical properties		Back contact	Front contact
	Electron & holes	1×10^{7}	1×10^{7}
	Work function	5.6286	4.4903
Allow contact tunneling	Relative to EF & E_C	0.0714 & -0.1227	0.0403 & 0.0019
	The effective mass of electrons & holes	1 and 1	1 and 1
Optical properties	Filter mode & value	Reflection & 0.8	Transmission & 0.95
	Complement of filter value	0.2	0.05

Ni, which realized a PCE of 23.39%. Alternative configurations, including $ZnSe/Sb_2Se_3$ and In_2S_3/Sb_2Se_3, exhibited 22.98% and 23.02% efficiencies, respectively. In contrast, the proposed configuration achieved remarkable results as shown in Table 4. This inquiry elucidates the advantages inherent in utilizing CIGS as an absorber layer instead of its Sb_2Se_3-based counterparts, exemplifying enhanced photovoltaic performance. Furthermore, the research accentuates the importance of optimizing material combinations to realize elevated efficiency levels. The outcomes of this study underscore the relevance of this novel configuration as a competitive and sustainable alternative for advancing thin-film solar cell technologies, thereby facilitating further optimization and practical application. Table 4 presents the difference between already presented work and previous work.

Figures (2-4) provide key insights into the performance and structure of CdS-based solar cells. Figure 2(a) shows the recombination curve, which highlights the rate at which charge carriers recombine within the solar cell, impacting efficiency. Figure 2(b) presents the I-V characteristic curve, essential for understanding the electrical behavior and efficiency of the solar cell under different operating conditions. Figure 3(a) illustrates the quantum efficiency (QE) curve, demonstrating the ability of the solar cell to convert incident photons into electrical current. Figure 3(b) depicts the photon energy curve, revealing the relationship between photon energy and the absorption efficiency of the solar cell. Lastly, Figure 4 displays the energy band diagram of the CdS-based solar cell, showing the alignment of energy levels across various layers, which is crucial for efficient charge carrier transport and overall device performance.

3.2. Impact of Absorber Layer Thickness

The absorber layer plays a vital role in solar cell performance for several reasons. It is the region where electron-hole pairs are primarily generated

Table 4. Comparison of this study with previous studies.

S. No.	Structure	V_{oc} (V)	J_{sc} (mA/cm^2)	FF (%)	PCE (%)
1	Ag/ZnO:Al/ZnO/CdS/Sb_2Se_3/Mo	0.43	32.17	62.20	8.72 [2]
2	CdS/Sb_2Se_3/Mo/Ni	0.78	35.45	84.14	23.39 [2]
3	ZnSe/Sb_2Se_3	0.78	35.41	82.70	22.98 [2]
4	In2S_3/Sb_2Se_3	0.78	35.19	83.41	23.02 [2]
5	Ag/ZnO:Al/ZnO/CdS/CIGS /Mo	0.795	35.93141	82.8	20.98 (This work)
6	Ag/ZnO:Al/ZnO/ZnSe/CIGS /Mo	0.705	35.93147	82.8	20.98 (This work)
7	Ag/ZnO:Al/ZnO/SnS_2/CIGS /Mo	0.7048	35.92011	83.04	21.02 (This work)
8	Ag/ZnO:Al/ZnO/SnS_2/CIGS /Mo	0.7049	35.959757	83	21.04 (This work)
9	Ag/ZnO:Al/ZnO/SnS_2/CIGS /Mo	0.7338	36.352805	83.33	22.23 (Optimized result)

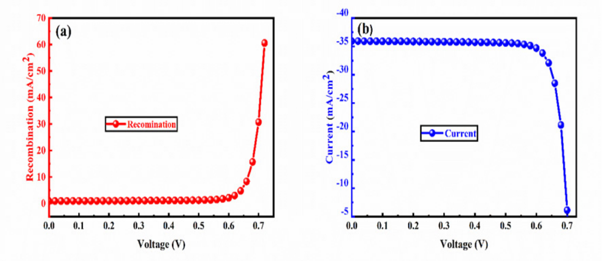

Fig. 2. (a) Recombination curve of CdS-based solar cell and (b) I-V characteristic curve of CdS-based solar cell.

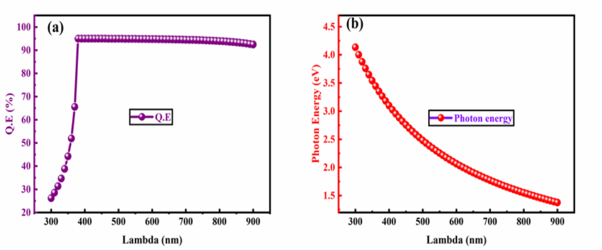

Fig. 3. (a) Quantum efficiency (QE) curve of CdS-based solar cell and (b) photon energy curve of CdS-based solar cell.

and constitutes a significant portion of the device's thickness. This characteristic is true for both silicon wafer and thin-film solar cell technologies. However, thin-film solar cells hold an advantage over wafer-based cells, as they can be much thinner and flexible, typically with thicknesses measured in microns. In contrast, wafer-based solar cells can be as thick as 200 µm [30]. To determine the optimal configuration, simulations were carried out using absorber layer thicknesses ranging from 2.0 to 4.0 µm, specifically analyzing the CIGS structure with a CdS buffer layer. Results indicated that increasing the thickness of the CIGS absorber layer enhances

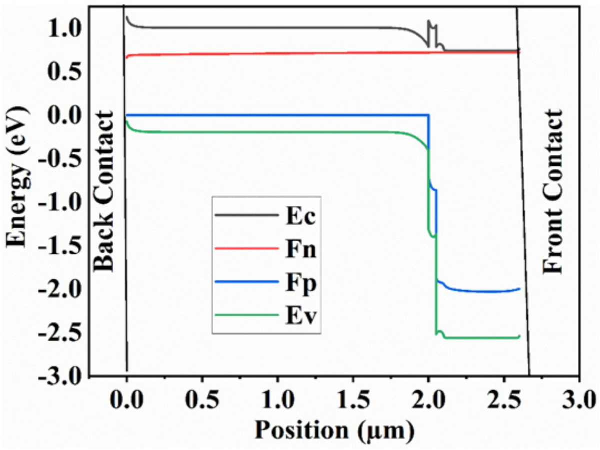

Fig. 4. Illustrating the alignment of energy levels across different layers.

the solar cell's efficiency. Key photovoltaic parameters, including short-circuit current density (J_{sc}), open-circuit voltage (V_{oc}), fill factor (FF), and power conversion efficiency (PCE) were evaluated as shown in Figure 5. Notably, J_{sc}, V_{oc}, and FF all improved with increasing absorber thickness, leading to higher overall efficiency. For example, J_{sc} increased from 35.93 mA/cm² to 36.1425 mA/cm² as the thickness rose from 2.0 to 4.0 µm, resulting in a corresponding efficiency improvement from 20.98% to 21.47%. This enhancement is largely due to improved photon absorption, especially for longer wavelengths, as the absorber layer becomes thicker [31]. Additionally, as seen in Figure 6(a), back contact recombination significantly decreases with greater absorber thickness, further boosting efficiency. Thicker absorber layers also increase the carrier diffusion length, which minimizes electron-hole pair losses at the rear contact and

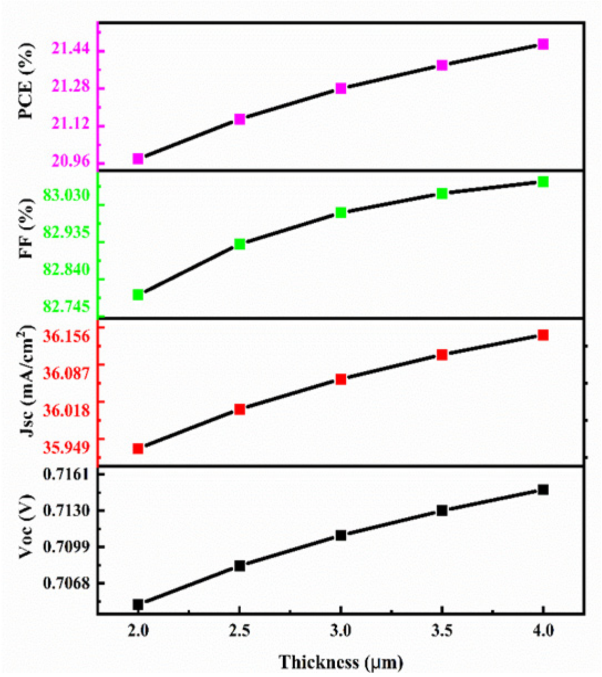

Fig. 5. Impact of absorber layer thickness on solar cell parameters such as V_{oc}, J_{sc}, FF (%), and PCE (%).

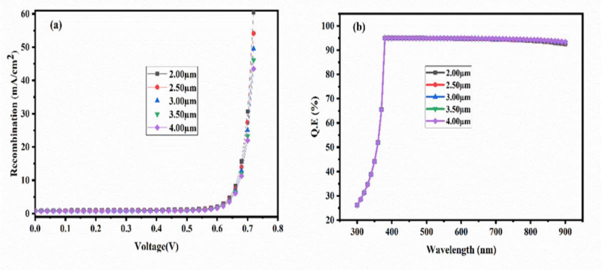

Fig. 6. (a) Recombination rate and (b) Quantum efficiency with varying absorber layer thickness.

contributes to better conversion efficiency [32]. However, extremely thin layers can exhibit quantum confinement effects, potentially altering the spectral response and introducing discrete energy levels [33]. Based on these findings, an absorber thickness of approximately 4.0 µm is considered optimal. Further increases in thickness offer minimal efficiency gains while requiring more material, making them less practical. Figure 6(b) illustrates how quantum efficiency (Q.E.) varies with absorber layer thickness.

3.3. Impact of Absorber Layer Acceptor Density

Our investigation analyzed the impact of acceptor density (N_A) on the performance of a p-type semiconductor material CIGS with a fixed thickness of 2 µm. The N_A concentration controlled the density of "holes" in the semiconductor material, affecting all key parameters of the solar cell [34]. We changed the majority carrier concentration within a range from 1×10^{16} to 1×10^{12} cm^{-3} and observed notable trends of different solar cell parameters in Figure 7. As the N_A changes from 1×10^{16} to 1×10^{12} cm^{-3}, the J_{sc} substantially rose from 35.93 to 36.32 mA/cm². Conversely, the V_{oc} showed an opposing behavior, decreasing from 0.705 to 0.6594 V during all the changes. Interestingly, N_A below 1×10^{15}, both V_{oc} and J_{sc} show little value changes. These findings underscore the critical role of acceptor concentration in determining device performance [35]. Notably, we observed a decline in FF and PCE when we changed the N_A values from 1×10^{16} to 1×10^{12} cm^{-3}. Careful deliberation of material suitability and reliability is essential to maintain optimal performance. There exists a trade-off between carrier concentration and recombination rates, where reduced acceptor concentration can lead to a decrease in carrier concentration, but if not properly controlled, may result in increased recombination, as shown in Figure 8. A decrease in the electrical conductivity due to reduced concentration of acceptors can impede charge separation and transport within the material, thus aiding in inefficient charge separation and transport [36]. Therefore, optimizing acceptor concentration can enhance the efficacy of thin-film solar cells by

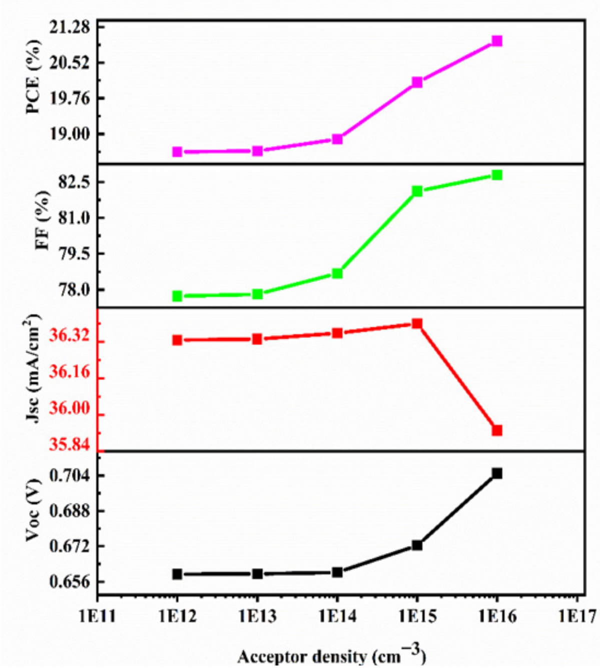

Fig. 7. Impact of acceptor density on solar cell parameters such as V_{oc}, J_{sc}, FF%, and PCE%.

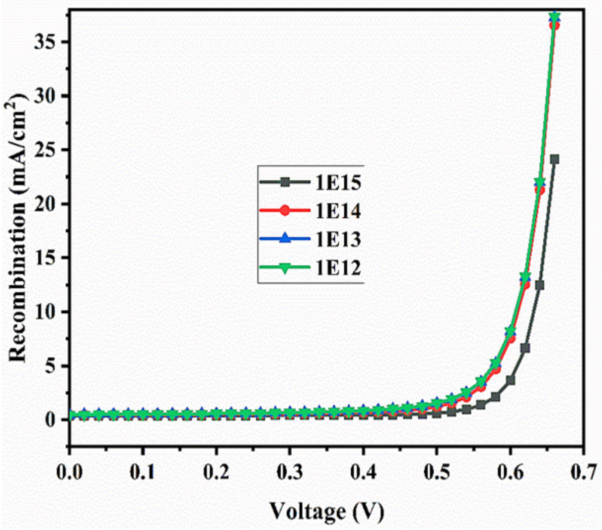

Fig. 8. Impact of accepter density on recombination rate.

dropping recombination rates of charge carriers, leading to higher overall PCE (%) and improving material stability and longevity.

3.4. Impact of Absorber Defects Density

We explored the impact of defect density (N_t) on the photovoltaic (PV) device performance. N_t is defined by the Shockley-Read-Hall recombination model by Equation (4):

$$R = \frac{np - n_i^2}{\tau_p \left(n + n_c e^{\left(E_g - E_\tau\right)/kT} \right) + \tau_p \left(p + n_v e^{\frac{(e_\tau)}{kT}} \right)} \quad (4)$$

Where, E_t shows trap energy levels, τ_p and τ_n are carrier lifetimes for holes and electrons, respectively [37]. Figure 9 illustrates the variations in essential PV parameters such as PCE (%), J_{sc}, FF, and V_{oc} with simultaneous changes in N_t. We varied N_t from 1×10^{18} to 1×10^{19} cm^{-3}, which shows that high N_t in the absorber layer is attributed to the poor quality of doping, notably in CGIS. Elevated N_t increases recombination rates due to pinhole formation, leading to reduced carrier diffusion lengths and diminished carrier collection efficiency at contacts, as shown in Figure 10. The drop in overall device performance is evident, and the increase in the N_t impacts the device's overall performance. PCE of PSCs substantially declines with increasing N_t, dropping from 20.98 to 4.23%. Similarly, FF decreases from 82.80 to 52.13%, with the same variations in N_t. J_{sc} and V_{oc} also show the same behavior as it decreases from 35.93 to 21.73 mA/cm^2 and 0.70 to 0.37 V variations with defect density values from 10^{15} cm^{-3} to 10^{19} cm^{-3}. Defect-induced impurities in the CIGS thickness or composition can lead to uneven light absorption across the solar cell's surface, ultimately reducing its overall PCE [38]. Because the defects can act as limiting factors, preventing the solar cell from achieving its maximum efficiency potential as described by the Shockley-Queisser limit [39]. The extent of these limitations depends on the type and

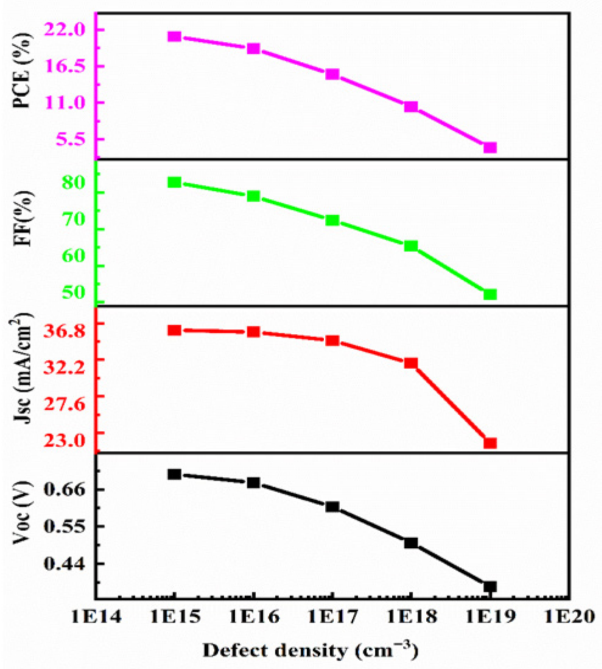

Fig. 9. Impact of absorber (N_t) on performance parameters.

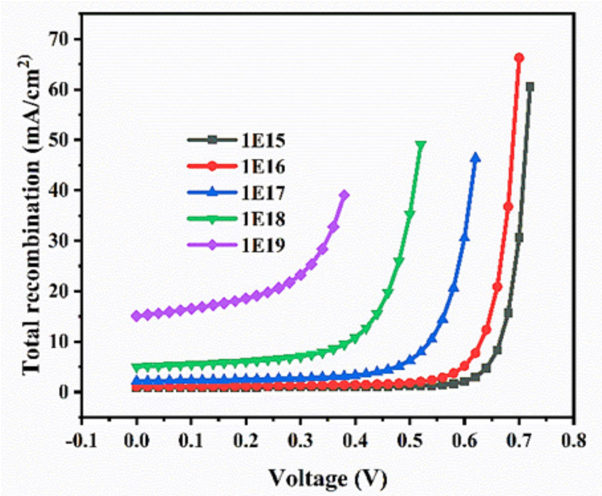

Fig. 10. Impact of absorber (N_t) on recombination rate.

density of defects present. To address these issues, researchers and engineers employ various strategies to modify the impact of defects. These approaches include interface engineering, defect passivation, and advancements in material growth techniques. By minimizing recombination and improving overall performance, these efforts aim to enhance the efficiency and effectiveness of solar cells.

3.5. Impact of Temperature

Temperature has a complex impact on the performance of thin-film solar cells, influencing parameters such as fill factor (FF), open-circuit voltage (Voc), short-circuit current density (Jsc), power conversion efficiency (PCE), and long-term durability [40]. Understanding these temperature effects is essential for optimizing the design and operation of solar cell systems, especially in environments with wide temperature variations. To explore these effects, simulations were conducted across a temperature range of 300 K to 320 K, as shown in Figure 11. This temperature range was selected to reflect realistic operating conditions while avoiding extreme scenarios that may introduce non-linear effects or material degradation beyond the scope of this study. One of the most significant temperature-related changes observed is the reduction in V_{oc} as temperature increases. This drop is attributed to the increase in intrinsic carrier concentration at elevated temperatures, which leads to higher recombination rates [41]. Due to this, fewer charge carriers reach the cell contacts, reducing the voltage output. In contrast, J_{sc} tends to show a modest increase with rising temperature. This is primarily due to improved charge carrier mobility, which enhances electrical conductivity and promotes more effective charge separation and transport. However, the slight gain in J_{sc} is typically insufficient to offset the loss in V_{oc}, ultimately resulting in a decrease in overall efficiency. Specifically, efficiency drops from 20.98% to 19.54% as temperature increases. This decline in performance is further linked to the temperature-dependent behavior of the semiconductor's bandgap. As temperature rises, the bandgap contracts, which causes the absorption spectrum to shift towards longer wavelengths. This reduces the cell's sensitivity to higher-energy photons and lowers the amount of electricity generated [42]. These findings are consistent with previous research and highlight the critical role of temperature in determining the efficiency and reliability of thin-film solar cells. Effectively understanding and mitigating temperature effects is essential for improving the performance and longevity of these devices under varying environmental conditions.

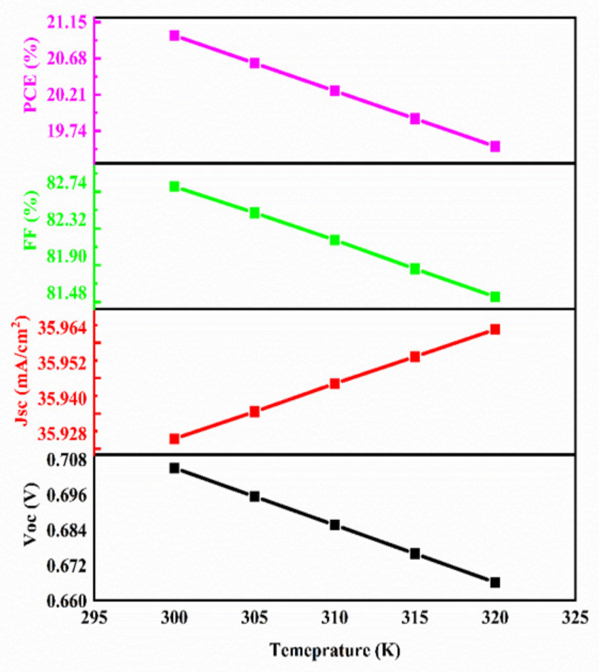

Fig. 11. Impact of temperature on solar cell parameters such as V_{oc}, J_{sc}, FF%, and PCE%.

3.6. Impact of Back Contact

The choice of back contact material (BCM) in thin-film solar cells significantly influences device performance; we used BCM such as Mo, Au, Cu, Pt, Pd, C, W, Ni, Se, and Fe [43]. Among these materials, the most widely utilized metal is molybdenum because of its efficiency and low cost, but in CIGS-based solar cells, Se BCM l shows superior efficiency. The performance of thin-film solar cells may be optimized by varying the work function value of the BCM. Simulation results, as depicted in Figure 12, illustrate a noticeable improvement in overall yield with changes in the BCM. This enhancement is attributed to the decline of recombination rates at the interface of BCM. When metal work function (MWF) increases the barrier height decreases, transforming the interface from Schottky to ohmic type [44]. Compared to molybdenum, an ohmic interface with an MWF of 5.9 eV facilitates improved charge carrier transport and extraction. The work function of the BCM directly impacts the energy barrier for charge

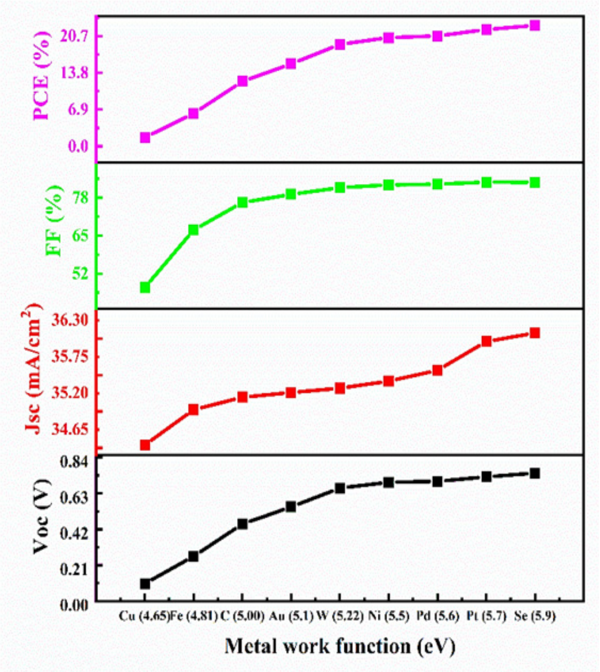

Fig. 12. Impact of back-metal work function on solar cell parameters.

carriers, inducing their ease of transportation and extraction. A suitable determined back contact MWF can boost charge carrier, increasing J_{sc} and 5.9 eV WF, showing this improvement in J_{sc} value from 35.93 to 36.40 mA/cm^2. Moreover, a suitable WF between the BCM and the semiconductor can minimize losses due to interface rejoining, resulting in a higher V_{oc}. A closely aligned work function is important in minimizing resistive losses and enhancing the movement of charge carriers within the solar cell [45]. Consequently, this alignment can result in a higher fill factor (FF) and increased power output. Careful selection of the metal used can optimize the FF(%), V_{oc}, and J_{sc}, mutually leading to enhanced inclusive PCE. Notably, efficiency has risen from 1.68 to 22.69% as the MWF ranges from 4.65 to 5.9 eV.

3.7. Impact of Cadmium-Free Buffer Layer

Cadmium-free photovoltaic cell structure and simulations offer an advanced and ecologically friendly method of utilizing solar energy [46]. In the present study, we substitute the Cds buffer layer with ZnSe, In_2S_3, and SnS_2 to improve thin-film photovoltaic modules' efficiency by using CIGS as an absorber material and the parameters outlined in Table.3 simulations were conducted, and results are depicted in Figure 13, with a summary of photovoltaic parameters in Table 5. Notably, the V_{oc} remains consistent across all buffer layers within the range of 0.7048 to 0.7050 V. However, J_{sc} shows a few variations with ZnSe, SnS_2, and In_2S_3 buffer layers approximately to 35.931, 35.92, and 35.959 mA/cm^2, respectively, because the In_2S_3 buffer layer has a wider bandgap, allowing more photons to reach the absorber, and offers better band alignment, reducing recombination losses and enhancing charge carrier collection. Fill factor analysis revealed SnS_2 exhibiting the highest value at 83.04%, while ZnSe displayed fill factors of 82.80, closely followed by CdS at 82.80%, and In_2S_3 showed an 83.00% value. CdS exhibited efficiency at 20.98%, ZnSe at 20.98%, In_2S_3 at 21.04%, and SnS_2 at 21.02%. These results indicate that cadmium-free buffer layers, specifically SnS_2 and In2S_3, perform comparably with CdS-based layers regarding fill factor. Whereas In_2S_3 still holds an efficiency advantage over CDs, alternatives demonstrate comparable high voltage, competitive fill factors, and J_{sc} values. The performance of ZnSe, In_2S_3, and SnS_2 as buffer layers compared to CdS can be attributed to their bandgaps, lattice matching, interface properties, and electronic characteristics, which collectively influence their effectiveness in enhancing the performance of thin-film solar cells. This is important for applications where environmental or toxicity concerns are a

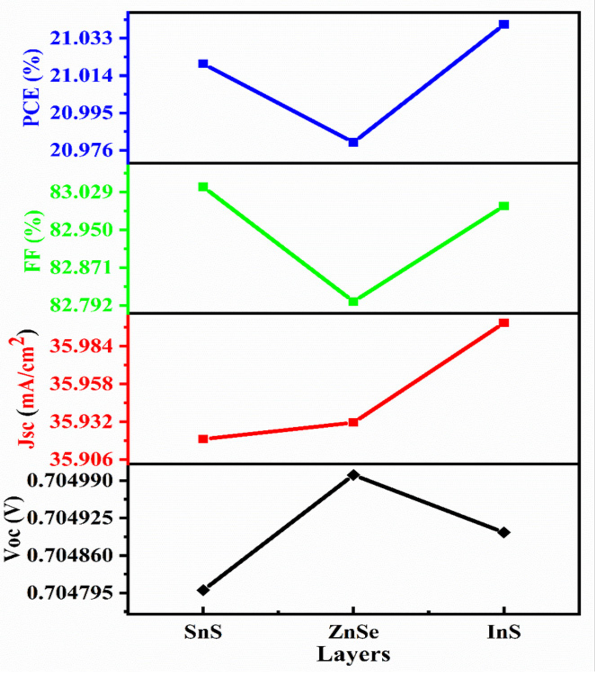

Fig. 13. Impact of different buffer layers on the cell's performance.

Table 5. Different buffer layers' impact performance.

S. No.	Buffer layer	V_{oc} (V)	J_{sc} (mA/cm^2)	FF (%)	PCE (%)
1	CdS	0.705	35.93141	82.8	20.98
2	ZnSe	0.705	35.93147	82.8	20.98
3	SnS_2	0.7048	35.92011	83.04	21.02
4	In_2S_3	0.7049	35.959757	83	21.04

priority. These alternatives show promise, offering similar or even better performance while avoiding toxic cadmium [47]. Figure 14 shows the impact of the buffer layer on Q.E%.

3.8. Impact of Different HTLs

To mitigate the limitations associated with expensive metals such as Se and Pt, a different layer referred to as the HTL is introduced between the absorber layer and the back contact. The HTL, typically a heavily doped p-type layer, serves to moderate the coalescing of minority carriers at the back contact [48, 49]. It is important to ensure the appropriate alignment of energy levels between the HTL material and the valence band of the absorber layer to facilitate effective hole removal. This alignment decreases the energy barrier for the whole movement, thus aiding in their movement across the interface HTL and absorber. Furthermore, factors such as refractive index and transparency are crucial considerations for the HTL. Transparency of the HTL permits incident light to enter and grasp the CIGS layer, while an optimal refractive index assists in minimizing optical losses and enhancing light trapping. Hence, HTL materials with a bandgap energy exceeding that of the absorber material are typically selected. For instance, in the present investigation, CuI and Spiro-MeOTAD were employed as HTL to evaluate their impact on the efficiency, and their bandgap values are 3.1 eV and 3.0 eV, respectively.

When employing HTL materials in thin-film solar cells to assess their impact on performance, observed changes in FF, PCE, J_{sc}, and V_{oc} can be attributed to several factors, and their J-V curve is presented in Figure 15. The decrease in FF and PCE from 82.8 to 71.63% and 20.98 to 19.32%, respectively, may result from increased resistive losses within the device or poor charge carrier collection efficiency due to inferior interface properties between the HTL and the absorber layer. Conversely, the increase in J_{sc} and V_{oc} from 35.93 to 36.20 mA/cm^2 and 0.705 to 0.7451 V, respectively, suggests improved charge carrier generation and extraction, possibly due to better alignment of energy levels between the absorber layer and HTL, leading to reduced energy barriers for carrier transport and enhanced device performance. These

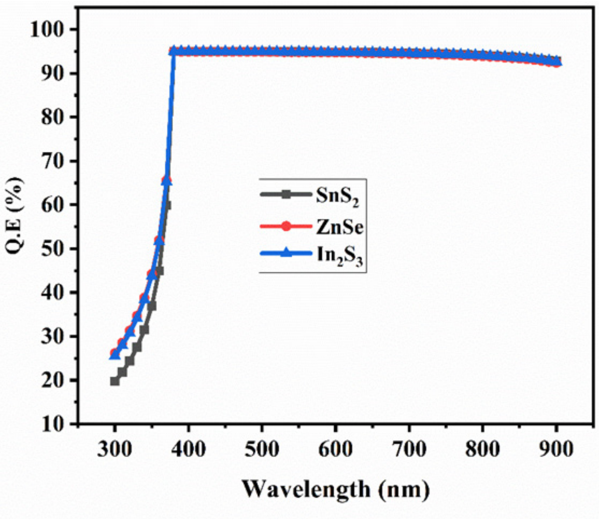

Fig. 14. Buffer layer impact on Q.E%.

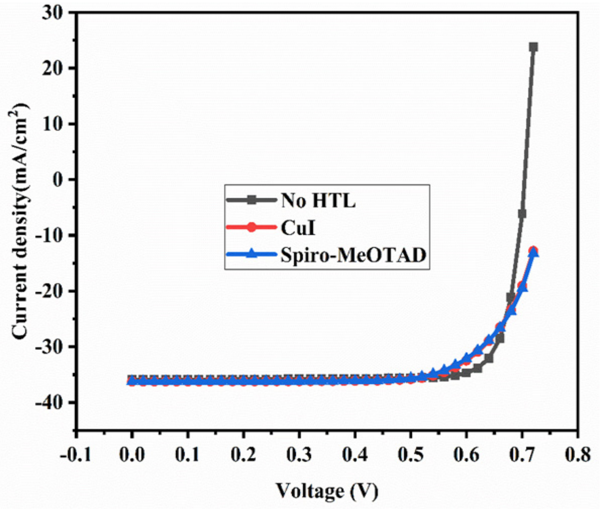

Fig. 15. Impact of different HTL on J-V curve.

outcomes underscore the intricate interplay between material properties, interface characteristics, and device architecture in determining the efficiency of thin-film solar cells employing CuI and Spiro-MeOTAD as HTL materials. Table 6 provides a summary of photovoltaic parameters for all cases. Therefore, precisely designed HTL layers are pivotal in optimizing thin-film solar cells' efficiency and dependability, making them a promising technology for sustainable energy production [50, 51].

Table 6. Performance comparisons between with and without HTL.

S. No.	Structure	V_{oc} (V)	J_{sc} (mA/cm^2)	FF (%)	PCE (%)
1	Without-HTL	0.705	35.93141	82.8	20.98
2	CuI	0.7451	36.20737	72.36	19.52
3	Spiro	0.7451	36.206	71.63	19.32

3.9. Simulation Optimization

In optimizing the solar cell structure, extensive analyses were performed on several key parameters to enhance its performance. Among these factors, the thickness of the absorber material and the work function of the metal, for instance, selenium (5.9 eV), are of significant importance. By carefully adjusting the thickness of the absorber layer, which in this case was 4.0 micrometers, significant improvements in the cell's efficacy and overall performance were achieved. These efforts have achieved a remarkable efficiency of 22.23% from 20.98% and show the importance of precise engineering at the material and structural levels, showcasing how targeted adjustments in these specific parameters can lead to substantial enhancements in solar cell efficiency. This optimization strategy emphasizes enhancing the solar cell's energy conversion efficiency while reducing material consumption and expenses. This ultimately aids in the progression of sustainable energy technologies.

4. CONCLUSIONS

This research has provided valuable insights into critical factors that influence solar cell efficiency based on CIGS technology. The study has underscored the intricate interplay of these variables in determining cell performance by systematically investigating the impact of absorber layer thickness, carrier concentration, buffer layers, HTLs, and back contact parameters. The optimization of absorber thickness demonstrated a crucial role in enhancing light absorption efficiency and charge carrier mobility while fine-tuning carrier concentration balanced carrier movement and recombination to achieve optimal performance. The work function of back contact metal was identified as a significant determinant of photovoltaic parameters, while temperature control strategies were highlighted as essential for reliable, highly efficient performance. The significant role of HTLs in mitigating recombination losses and enhancing charge collection was explored, with notable efficiency reductions observed when substituting CdS with alternative HTLs such as CuI (19.52%) and Spiro-MeOTAD (19.32%). A promising pathway toward environmentally friendly solar cells was emphasized by using In_2S_3 as a cadmium-free buffer layer, achieving an impressive efficiency of 22.23% after optimization. These findings reinforce the potential of CIGS technology as a cost-effective and sustainable energy solution capable of addressing the growing demand for renewable energy sources. The study highlights the importance of careful design and parameter optimization and lays a strong foundation for future advancement in CIGS-based solar cells. Continued research in developing cadmium-free designs and refining fabrication techniques will be instrumental in overcoming the remaining challenges. These efforts promise to improve further the efficiency, scalability, and environmental sustainability of CIGS solar cells, thus advancing the global transition toward cleaner and more reliable energy systems.

5. CONFLICT OF INTEREST

The authors have no conflict of interest to disclose.

6. REFERENCES

1. F. Qin, Y. Zhang, K. Naseem, Z. Chen, G. Suo, W. Hayat, and S.H.S. Gardezi. Assessment of the importance and catalytic role of chromium oxide and chromium carbide for hydrogen generation via hydrolysis of magnesium. *Nanoscale* 16(41): 19518-19528 (2024).
2. F. Qin, K. Naseem, Z. Chen, G. Suo, and A. Tahir. Carbon nano-tube coated with iron carbide catalysis for hydrolysis of magnesium to generate hydrogen. *International Journal of Hydrogen Energy* 83:

1359-1369 (2024).

3. K. Naseem, H. Zhong, W. Jiang, M. Liu, C. Lang, K. Chen, L. Ouyang, and J. Huang. A reusable dual functional Mo₂C catalyst for rapid hydrogen evolution by Mg hydrolysis. *Journal of Materials Chemistry A* 11(36): 19328-19337 (2023).
4. E. Kabir, P. Kumar, S. Kumar, A.A. Adelodun, and K.-H. Kim. Solar energy: Potential and future prospects. Renewable and Sustainable. *Energy Reviews* 82: 894-900 (2018).
5. S. Moujoud, B. Hartiti, S. Touhtouh, F. Belhora, and A. Hajjaji. Optimizing Sb_2Se_3 thin-film solar cells: A comprehensive simulation study of multiple influential factors. *Optik* 303: 171723 (2024).
6. O.J. Olujobi, U.E. Okorie, E.S. Olarinde, and A.D. Aina-Pelemo. Legal responses to energy security and sustainability in Nigeria's power sector amidst fossil fuel disruptions and low carbon energy transition. *Heliyon* 9: e17912 (2023).
7. A.A. Hussien, A.A. Salem, S.W. Sharshir, and T. Nabil. Performance Assessment of an Automated Hybrid Solar Desalination System Powered by Solar PV and Wind Turbine: Experimental Investigation. *SSRN 4766771* (2024). https://papers.ssrn.com/sol3/papers.cfm?abstract_id=4766771
8. Y. Kim, M. Shin, M. Lee, and Y. Kang. Hot-spot generation model using electrical and thermal equivalent circuits for a copper indium gallium selenide photovoltaic module. *Solar Energy* 216: 377-385 (2021).
9. S.R. Fatemi Shariat Panahi, A. Abbasi, V. Ghods, and M. Amirahmadi. Analysis and improvement of CIGS solar cell efficiency using multiple absorber substances simultaneously. *Journal of Materials Science*: *Materials in Electronics* 31: 11527-11537 (2020).
10. L. Lin and N.M. Ravindra. CIGS and perovskite solar cells–an overview. *Emerging Materials Research* 9: 812-824 (2020).
11. H.I. Abdalmageed, M. Fedawy, and M.H. Aly. Effect of absorber layer bandgap of CIGS-based solar cell with (CdS/ZnS) buffer layer. *Journal of Physics: Conference Series* 2128: 012009 (2021).
12. M. Islam, T. Ahmed, S.U.D. Shamim, A.A. Piya, and A. Basak. Thickness dependent numerical investigations of lead-free perovskite/CIGS bilayer solar cell using SCAPS-1D. *Chemistry of Inorganic Materials* 2: 100034 (2024).
13. A.N. Das, P.K. Paul, M.H. Jewel, A.A. Mamun, K.H. Akhand, and S.A. Chowdhury. Analytical Modeling and Performance analysis of Copper-Indium-Gallium-Di Selenide-Based (CIGS) Solar Cell by SCAPS-1D. *7th International Conference on Development in Renewable Energy Technology (ICDRET)* pp. 1-6 (2024).
14. B.F. Gonçalves, S. Sadewasser, L.M. Salonen, S. Lanceros-Méndez, and Y.V. Kolen'ko. Merging solution processing and printing for sustainable fabrication of Cu (In, Ga) Se_2 photovoltaics. *Chemical Engineering Journal* 442: 136188 (2022).
15. M. Burgelman, K. Decock, S. Khelifi, and A. Abass. Advanced electrical simulation of thin film solar cells. *Thin Solid Films* 535: 296-301 (2013).
16. M.F. Hossain, A. Ghosh, M.A.A. Mamun, A.A. Miazee, H. Al-lohedan, R.J. Ramalingam, M.F. Islam Buian, S.R.I. Karim, M.Y. Ali, and M. Sundararajan. Design and simulation numerically with performance enhancement of extremely efficient Sb_2Se_3-Based solar cell with V_2O_5 as the hole transport layer, using SCAPS-1D simulation program. *Optics Communications* 559: 130410 (2024).
17. E. Danladi, P.M. Gyuk, N.N. Tasie, A.C. Egbugha, D. Behera, I. Hossain, I.M. Bagudo, M.L. Madugu, and J.T. Ikyumbur. Impact of hole transport material on perovskite solar cells with different metal electrode: a SCAPS-1D simulation insight. *Heliyon* 9: e14326 (2023).
18. M. Zakir Muzakkar, N.A. Busri, A.A. Umar, L.O.A. Salim, Maulidiyah, and M. Nurdin. Enhanced Performance of Perovskite Solar Cells with Tungsten-Doped SnO₂ as an Electron Transport Material. *Journal of Inorganic and Organometallic Polymers and Materials* 1-9 (2024).
19. A.R. Smith, M. Ghamari, S. Velusamy, and S. Sundaram. Thin-Film Technologies for Sustainable Building-Integrated Photovoltaics. *Energies* 17(24): 6363 (2024).
20. C.J. Petti, M.M. Hilali, and G. Prabhu. Thin Films in Photovoltaics. In: Handbook of Thin Film Deposition: Techniques, Processes, and Technologies. K. Seshan (Ed.). *Elsevier* pp. 313-359 (2012).
21. A. ul Rehman, T. Munir, S. Afzal, M. Saleem, and I.L. Ikhioya. Enhanced Solar Cell Efficiency with Tin-Based Lead-Free Material (FASnI3) through SCAPS-1D Modeling. *Eurasian Journal of Science and Technology* 4: 258-263 (2024).
22. N. Khoshsirat, N.A.M Yunus, M.N. Hamidon, S. Shafie, and N. Amin. Analysis of absorber and buffer layer band gap grading on CIGS thin film solar cell performance using SCAPS. *Pertanika Journal of Science and Technology* 23(2): 241-250 (2015).
23. M.K. Hossain, M.K.A. Mohammed, R. Pandey,

A.A. Arnab, M.H.K. Rubel, K.M. Hossain, M.H. Ali, M.F. Rahman, H. Bencherif, J.V. Madan, M.R. Islam, D.P. Samajdar, and S. Bhattarai. Numerical analysis in DFT and SCAPS-1D on the influence of different charge transport layers of CsPbBr3 perovskite solar cells. *Energy & Fuels* 37: 6078–6098 (2023).

24. A.K. Chaudhary, S. Verma, and R.K. Chauhan. Thermal and power performance optimization of cost-effective solar cells using eco-friendly perovskite materials. *Physica Scripta* 99: 025512 (2024).
25. Z. Qiu, Y. Li, X. Long, H. Tian, Y. Pu, B. Lv, J. Wei, Q. Dai, and W. Wang. Built-in electric field induced efficient interfacial charge separation via the intimate interface of CdS-based all-sulfide binary heterojunction for enhanced photoelectrochemical performance. *Journal of Alloys and Compounds* 976: 173188 (2024).
26. M.F. Rahman, M. Chowdhury, L. Marasamy, M.K.A. Mohammed, M.D. Haque, S.R.A. Ahmed, A. Irfan, A.R. Chaudhry, and S. Goumri-Said. Improving the Efficiency of a CIGS Solar Cell to Above 31% with Sb_2S_3 as a New BSF: A Numerical Simulation Approach by SCAPS-1D. *RSC Advances* 14(3): 1924-1938 (2024).
27. S.H. Zyoud, A.H. Zyoud, N.M. Ahmed, and A.F.I. Abdelkader. Numerical modelling analysis for carrier concentration level optimization of CdTe heterojunction thin film–based solar cell with different non–toxic metal chalcogenide buffer layers replacements: using SCAPS–1D software. *Crystals* 11: 1454 (2021).
28. T.D. Lee and A.U. Ebong. A review of thin film solar cell technologies and challenges. *Renewable and Sustainable Energy Reviews* 70: 1286–1297 (2017).
29. F. Elhady, T.M. Abdolkader, and M. Fedawy. Simulation of new thin film Zn (O, S)/CIGS solar cell with bandgap grading. *Engineering Research Express* 5: 025027 (2023).
30. M.K. Hossain, G.F.I. Toki, I. Alam, R. Pandey, D.P. Samajdar, M.F. Rahman, M.R. Islam, M.H.K. Rubel, H. Bencherif, J. Madan, and M.K.A. Mohammad Numerical simulation and optimization of a CsPbI$_3$-based perovskite solar cell to enhance the power conversion efficiency. *New Journal of Chemistry* 47: 4801-4817 (2023).
31. A.K. Ogundele and G.T. Mola. Semiconductor quantum dots as a mechanism to enhance charge transfer processes in polymer solar cells. *Chemosphere* 345: 140453 (2023).
32. I. Chabri, Y. Benhouria, A. Oubelkacem, A. Kaiba, I. Essaoudi, and A. Ainane. SCAPS device simulation study of formamidinium Tin-Based perovskite solar cells: Investigating the influence of absorber parameters and transport layers on device performance. *Solar Energy* 262: 111846 (2023).
33. N.A.Z. Abidin, F. Arith, N.S. Noorasid, H. Sarkawi, A.N. Mustafa, N.E. Safie, A.S. Mohd Shah, M.A. Azam, P. Chelvanathan, and N. Amin. Dopant engineering for ZnO electron transport layer towards efficient perovskite solar cells. *RSC Advances* 13: 33797-33819 (2023).
34. K. Liang, L. Huang, T. Wang, C. Wang, Y. Guo, Y. Yue, X. Liu, J. Zhang, Z. Hu, and Y. Zhu. Rational design of formamidine tin-based perovskite solar cell with 30% potential efficiency via 1-D device simulation. *Physical Chemistry Chemical Physics* 25: 9413-9427 (2023).
35. K.D. Jayan. Design and Comparative Performance Analysis of High-Efficiency Lead-Based and Lead-Free Perovskite Solar Cells. *Physica Status Solidi (a)* 219: 2100606 (2022).
36. Y. Ming, H. Wang, W. Cai, and Z. Zang. Mixed-Halide Inorganic Perovskite Solar Cells: Opportunities and Challenges. *Advanced Optical Materials* 11: 2301052 (2023).
37. M. Jihyun, Y. Choi, D. Kim, and T. Park. Beyond Imperfections: Exploring Defects for Breakthroughs in Perovskite Solar Cell Research. *Advanced Energy Materials* 14: 2302659 (2024).
38. A. Rehman, S. Afzal, I. Naeem, D. Bibi, S.G. Sarwar, F. Nabeel, and R.M. Obodo. Performance Optimization of FASnI$_3$ Based Perovskite Solar Cell Through SCAPS-1D Simulation. *Hybrid Advances* 7: 100301 (2024).
39. L.C. Ghosekar and G.C. Patil. Performance analysis and thermal reliability study of multilayer organic solar cells. *IEEE Transactions on Device and Materials Reliability* 19: 572-580 (2019).
40. S. Priyanka and N.M. Ravindra. Temperature dependence of solar cell performance - an analysis. *Solar Energy Materials and Solar Cells* 101: 36-45 (2012).
41. R.L. Milot, G.E. Eperon, H.J. Snaith, M.B. Johnston, and L.M. Herz. Temperature-dependent charge-carrier dynamics in CH$_3$NH$_3$PbI$_3$ perovskite thin films. *Advanced Functional Materials* 25: 6218-6227 (2015).
42. J.K. Deepthi and V. Sebastian. Comprehensive device modelling and performance analysis of MASnI$_3$ based perovskite solar cells with diverse ETM, HTM and back metal contacts. *Solar Energy* 217: 40-48 (2021).

43. A. Rehman, M. Iqbal, D. Bibi, F. Muneer, S. Afzal, T. Munir, and M. Bilal. Optimization of Lead-Free Inorganic Perovskite Solar Cells: SCAPS Numerical Simulation Study on $(FA)_2BiCuI_6$ Absorber Layer. *Eurasian Journal of Science and Technology* 4(4): 340-354 (2024).
44. D. Wang, J. Sheng, S. Wu, J. Zhu, S. Chen, P. Gao, and J. Ye. Tuning back contact property via artificial interface dipoles in Si/organic hybrid solar cells. *Applied Physics Letters* 109(4): 043901 (2016).
45. M. Bivour, J. Temmler, F. Zähringer, S. Glunz, and M. Hermle. High work function metal oxides for the hole contact of silicon solar cells. *IEEE 43rd Photovoltaic Specialists Conference (PVSC), Portland, OR, USA* pp. 0215-0220 (2016).
46. T. Ibn-Mohammed, S.C.L. Koh, I.M. Reaney, A. Acquaye, G. Schileo, K.B. Mustapha, and R. Greenough. Perovskite solar cells: An integrated hybrid lifecycle assessment and review in comparison with other photovoltaic technologies. *Renewable and Sustainable Energy Reviews* 80: 1321-1344 (2017).
47. K. Vijayan, S.P. Vijayachamundeeswari, K. Sivaperuman, N. Ahsan, T. Logu, and Y. Okada. A review on advancements, challenges, and prospective of copper and non-copper based thin-film solar cells using facile spray pyrolysis technique. *Solar Energy* 234: 81-102 (2022).
48. F.S. Ahmadpanah, A.A. Orouji, and I. Gharibshahian. Improving the efficiency of CIGS solar cells using an optimized p-type CZTSSe electron reflector layer. *Journal of Materials Science: Materials in Electronics* 32(17): 22535-22547 (2021).
49. I. Gharibshahian, A.A. Orouji, and S. Sharbati. Effectiveness of band discontinuities between CIGS absorber and copper-based hole transport layer in limiting recombination at the back contact. *Materials Today Communications* 33: 104220 (2022).
50. P. Chelvanathan, M.I. Hossain, and N. Amin. Performance analysis of copper–indium–gallium–diselenide (CIGS) solar cells with various buffer layers by SCAPS. *Current Applied Physics* 10(3): S387-S391 (2010).
51. M. Islam, T. Ahmed, S.U.D. Shamim, A.A. Piya, and A. Basak. Thickness dependent numerical investigations of lead-free perovskite/CIGS bilayer solar cell using SCAPS-1D. *Chemistry of Inorganic Materials 2*: 100034 (2024).